Available online at www.sciencedirect.com

ScienceDirect

journal homepage: www.elsevier.com/locate/he

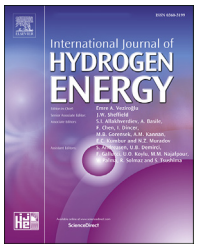

Promotion effect of proton-conducting oxide $BaZr_{0.1}Ce_{0.7}Y_{0.2}O_{3-\delta}$ on the catalytic activity of Ni towards ammonia synthesis from hydrogen and nitrogen

John Humphreys [a], *Rong Lan* [a,c], *Dongwei Du* [a], *Wei Xu* [a], *Shanwen Tao* [a,b,*]

[a] *School of Engineering, University of Warwick, Coventry, CV4 7AL, UK*
[b] *Department of Chemical Engineering, Monash University, Clayton, Victoria, 3800, Australia*
[c] *Faculty of Engineering, Environment & Computing, Coventry University, Coventry, CV1 5FB, UK*

ARTICLE INFO

Article history:
Received 26 April 2018
Received in revised form
30 July 2018
Accepted 1 August 2018
Available online 23 August 2018

Keywords:
Renewable hydrogen
Ammonia synthesis
Catalysis
Proton conductor
Nickel catalyst
Catalyst promoter

ABSTRACT

In this report, for the first time, it has been observed that proton-conducting oxide $BaZr_{0.1}Ce_{0.7}Y_{0.2}O_{3-\delta}$ (BZCY) has significant promotion effect on the catalytic activity of Ni towards ammonia synthesis from hydrogen and nitrogen. Renewable hydrogen can be used for ammonia synthesis to save CO_2 emission. By investigating the operating parameters of the reaction the optimal conditions for this catalyst were identified. It was found that at 620 °C with a total flow rate of 200 mL min^{-1} and a H_2/N_2 mol ratio of 3, an activity of approximately 250 μmol g^{-1} h^{-1} can be achieved. This is ten times larger than that for the unpromoted Ni catalyst under the same conditions although the stability of both catalysts in the presence of steam was not good. The specific activity of Ni supported on proton-conducting oxide BZCY is approximately 72 times higher than that of Ni supported on non-proton conductor MgO–CeO_2. These promotion effects were suspected to be due to the proton conducting nature of the support. Therefore it is proposed that the use of proton conducting support materials with highly active ammonia synthesis catalysts such as Ru and Fe will provide improved activity of at lower temperatures.

Introduction

Ammonia, due to its important use as a fertiliser is mass produced at approximately 150 million tons per annum [1]. That fact that ammonia fertilisers have supported approximately 27% of the world's population over the last century confirms its importance, with the development of the high temperature Haber-Bosch process being considered one of the most important chemical processes of the last 100 years [2]. In this process, ammonia is produced from H_2 and N_2 under high temperature and high pressure. About 50% of the hydrogen produced in the world is used for ammonia production [3]. In addition, CO_2 emitted from the ammonia industry is equivalent to 0.77% of the world total CO_2 emission because the

* *Corresponding author*. School of Engineering, University of Warwick, Coventry, CV4 7AL, UK.
E-mail address: S.Tao.1@warwick.ac.uk (S. Tao).
https://doi.org/10.1016/j.ijhydene.2018.08.002

source of hydrogen is mainly from steam-reforming of natural gas [3,4]. This green-house gas emission can be significantly reduced if the source of hydrogen can be changed to be provided through renewable sources such as hydro-electricity, wind or solar energy. Hydrogen from the electrolysis of water (hydroelectricity) was used for low-carbon ammonia production through Haber-Bosch process in Norway [5]. A Dutch company Proton Venture is developing de-centralised ammonia production technology using renewable electricity as the energy source [6]. Therefore synthesis of ammonia from renewable hydrogen could be a complementary part of hydrogen economy [3,7–11].

The Haber-Bosch process is very important in chemical industry. This led to Fritz Haber being awarded the Nobel Prize in 1918 and with Carl Bosch also receiving the award in 1931. Gerhard Etrl also won the Nobel Prize in Chemistry in 2007 for his contributions towards the understanding of the surface chemistry of iron catalyst [12]. Industrially promoted fused iron catalysts are used in the Haber-Bosch process with promoters including potassium, barium and aluminium oxides [13–18]. As well as iron, supported ruthenium has attracted a large amount of research interest as an ammonia synthesis catalyst with carbon supported ruthenium currently employed in the Kellogg advanced ammonia process (KAAP) [19]. Due to the cost of ruthenium, it is supported on a range of materials in order to be used in the ammonia synthesis process. These supports often also fill the role of promoter with very high activities recently reported for Ru/HT-C12A7:e^- [20], Ru/Y_5Si_2 [21], and Ru/MgO [22] supports. In 2013 Wang Z et al. [23] reported the use of perovskite material $BaZrO_3$ as a catalyst support for the ammonia synthesis reaction at high pressure and intermediate temperature when ruthenium was used as the catalyst.

The reaction to produce ammonia from hydrogen is shown below [19].

$$N_2 + 3H_2 \leftrightarrow 2NH_3 \ (\Delta H^o = -46.1\ kJ\ mol^{-1}) \quad (1)$$

Although this reaction is exothermic and favours high pressure and low temperature the ammonia formation rate at these conditions is extremely low even though an ammonia equilibrium concentration of close to 100% is theoretically possible. For this reason, the Haber-Bosch process is carried out at temperatures between 400 °C and 500 °C at pressures close to 200 bar.

It is commonly accepted that the rate limiting step for the ammonia synthesis reaction is the dissociative adsorption of nitrogen although the reaction could also be limited by the N binding energy due to the Sabatier principle [24]. This is shown in Eqs (2)–(8) below:

$$N_2 + {}^* \leftrightarrow N_2^* \quad (2)$$

$$N_2^* + {}^* \leftrightarrow 2N^* \quad (3)$$

This dissociated nitrogen reacts with dissociated hydrogen on the catalyst surface to form ammonia. The dissociative adsorption of hydrogen and the surface reactions are shown below where * represents the catalyst active site:

$$H_2 + 2^* \leftrightarrow 2H^* \quad (4)$$

$$H^* + N^* \leftrightarrow NH^* + {}^* \quad (5)$$

$$NH^* + H^* \leftrightarrow NH_2^* + {}^* \quad (6)$$

$$NH_2^* + H^* \leftrightarrow NH_3^* + {}^* \quad (7)$$

$$NH_3^* \leftrightarrow NH_3 + {}^* \quad (8)$$

It can be seen from this that if the dissociative adsorption of hydrogen is favoured on the catalyst surface then there will be less active sites for the rate limiting step therefore reducing activity. It has been reported that reduce dinitrogen will be feasible upon addition of protons and electrons similar to the mechanism of ammonia production by nitrogenases. This has been described in detail in an excellent review [25].

Recently, it was discovered that ammonia could be produced from hydrogen and nitrogen in an electrochemical cell [7,26–35]. This led Vasileiou E et al. [36,37] to achieve the electrochemical synthesis of ammonia using a proton conducting electrolyte. They achieved this by using $BaCe_{0.2}Zr_{0.7}Y_{0.1}O_{2.9}$ as the electrolyte with Ni–$BaCe_{0.2}Zr_{0.7}Y_{0.1}O_{2.9}$ used as the cathode and anode. When they performed the experiment with no applied voltage they discovered that ammonia was also produced through the catalysed reaction of H_2 and N_2 fed to the cell. Although the catalytic activity of the Ni–$BaCe_{0.2}Zr_{0.7}Y_{0.1}O_{2.9}$ material was noted no further investigation was done. In this paper, the effects of a similar proton conducting electrolyte on the catalytic activity towards ammonia synthesis, were investigated with the use of a Ni catalyst. $BaZr_{0.1}Ce_{0.7}Y_{0.2}O_{3-\delta}$ (BZCY) was chosen due to its excellent proton conductivity [38,39]. Ni-BZCY has been investigated as membrane materials for hydrogen separation using the proton conduction of BZCY [40,41]. By using a proton conducting support, it is proposed that the dissociated hydrogen on the catalyst active sites will be transferred to the proton conducting support, therefore freeing active sites for the dissociative adsorption of nitrogen. Through this increase in active sites, it is expected that the catalyst activity will be greatly increased. In this study, the catalytic activity of Ni and Ni supported on BZCY or MgO–CeO_2 are investigated. It was found that proton-conducting oxide BZCY has promotion effects on the catalytic activity towards ammonia synthesis.

Experimental

Materials and preparation method

In order to synthesise the $BaZr_{0.1}Ce_{0.7}Y_{0.2}O_{3-\delta}$ (BZCY) perovskite catalyst support a solid state reaction was employed. Firstly stoichiometric amounts of $BaCO_3$ (99% alfa), ZrO_2 (99% alfa), CeO_2 (99.5% Alfa) and Y_2O_3 (99.9% Alfa) were weighed and mixed using a pestle and mortar. The resulting mixture was then wet ground in isopropyl alcohol for 12 h. After drying at 80 °C the mixture was then fired at 1000 °C for 3 h with a heating and cooling rate of 5 °C min^{-1}. After this NiO (99% Alfa) was added to the $BaZr_{0.1}Ce_{0.7}Y_{0.2}O_3$

powder with a weight ratio of 60%–40% respectively. This was further wet ground in isopropyl alcohol for 12 h. The MgO–CeO_2 support for the comparison test was prepared through a combustion synthesis in which equimolar amounts of $Ce(NO_3)_3$ $6H_2O$ (99.5% alfa) and $Mg(NO_3)_2$ $6H_2O$ (98% alfa) were dissolved in deionised water, citric acid (99% alfa) was then added with the mole ratio of 1:1 against total moles of metal ions. This solution was then heated on a hot plate at 200 °C until the combustion was complete with the resulting powder fired at 500 °C for 2 h. After this NiO (99% Alfa) was added to the MgO–CeO_2 powder with a weight ratio of 60%–40% respectively. This was further wet ground in isopropyl alcohol for 12 h.

Materials characterisation

The catalyst was characterised using both X-ray Diffraction (XRD) and Scanning electron microscopy (SEM). The crystal structures were determined using a Panalytical X'Pert Pro Multi-Purpose Diffractometer (MPD) with Cu K alpha 1 radiation working at 45 kV and 40 mA. The SEM images were obtained with ZEISS SUPRA 55-VP operating at 10 kV. Thermalgravimetry-differential scanning calorimetry (TG-DSC) analyses of pre-reduced Ni-BZCY catalysts were carried out on a NETSCH STA 449 F1 thermal analyser in flowing N_2 to 800 °C with an N_2 flowing rate of 70 mL min^{-1} [35]. FT-IR measurements were carried out on a Bruker Vertex 70V IR spectrometer. The specific surface area of both the Ni-BZCY catalyst and the Ni–MgO–CeO_2 catalyst was measured using a QUADRASORB SI surface area analyser. Both of the reduced samples were degassed at 350 °C before carrying out surface area analysis at liquid nitrogen temperature.

Catalyst activity measurement

To measure the catalytic activity 0.48 g of catalyst was loaded into an alumina reactor and was supported in the centre on glass fibre. The catalyst was then reduced at 700 °C in H_2 and N_2 with a total flow rate of 100 mL min^{-1} and mole ratio of 9:1 H_2:N_2 for 4 h. After this the temperature, total flow rate and flow rate ratio were adjusted in order to determine the optimal conditions. H_2 and N_2 from gas cylinders were directly used without any purification process. For the stability test, the catalyst was cooling down to room temperature under the protection of mixed H_2/N_2 (3:1 m/o), then N_2 passing through room temperature water was passed through the catalyst for one hour. After this process, the gas was switched to mixed H_2 and N_2 then slowly heated to 620 °C to continue the ammonia synthesis measurement.

Dilute H_2SO_4 (0.01 M) was used to collect any produced ammonia which was then measured using ISE Thermo Scientific Orion Star A214 ammonia meter. Both hydrogen and nitrogen were used from the cylinder with no further purification.

In order to calculate the ammonia synthesis rate the following equation was used.

$$r_{NH_3} = \frac{[NH_4^+] \times V}{t \times m} \quad (9)$$

where $[NH^+_4]$ is ammonia concentration in mol L^{-1}, V is volume of 0.01 M H_2SO_4 in L, t is time in hours and m is catalyst mass in g.

Results and discussion

Materials characterisation

XRD analyses

In the XRD results shown in Fig. 1, it can be seen that there are some small peaks attributed to $BaCO_3$ and Y-doped $Ce_xZr_{1-x}O_2$ present for $BaZr_{0.1}Ce_{0.7}Y_{0.2}O_{3-\delta}$ before and after being mixed with the NiO; however, after reduction at 700 °C in H_2/N_2 mixture (90%H_2) for 4 h, these peaks are no longer present. A possible reason is that, $BaCO_3$ and Y-doped $Ce_xZr_{1-x}O_2$ were converted into amorphous phase during the reduction process thus cannot be detected by XRD. The XRD peaks for the catalyst before and after the stability test are the same although the intensity of the Ni peak has increased after the stability tested showing the possible aggregation of Ni particles whilst better crystallisation is another possible reason.

FT-IR analysis

In order to identify the $BaCO_3$ phase, the absorbance spectra of the catalyst were measured before and after reduction to investigate whether or not $BaCO_3$ and Y-doped $Ce_xZr_{1-x}O_2$ are converted into amorphous phases. The absorbance spectra of pure $BaCO_3$, ZrO_2, CeO_2 and the catalysts before and after catalysts test were measured using a Bruker Vertex 70V IR spectrometer. FT-IR was employed over the wavenumber range of 500 cm^{-1} to 4000 cm^{-1}. Fig. 2 shows that the adsorption for $BaCO_3$ at around 1440 cm^{-1} were present in both the reduced and unreduced catalyst, remaining present in an amorphous phase throughout the catalyst tests. The observed IR adsorption for $BaCO_3$ is consistent with that in a previous report [42]. It has been reported that a similar perovskite oxide to BZCY, $BaZr_{0.8}Y_{0.2}O_{3-\delta}$ does not exhibit adsorption around this wavenumber [43]. It was noticed that the adsorption peak for $BaCO_3$ at approximately 1250 cm^{-1} is

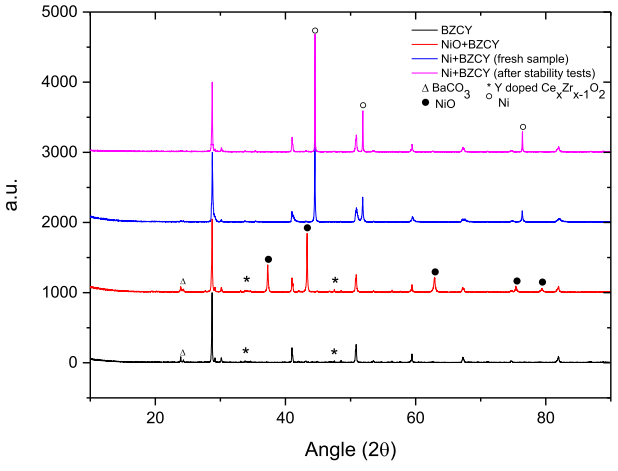

Fig. 1 – XRD images of the BZCY proton conducting support and the supported Ni catalyst before and after stability test.

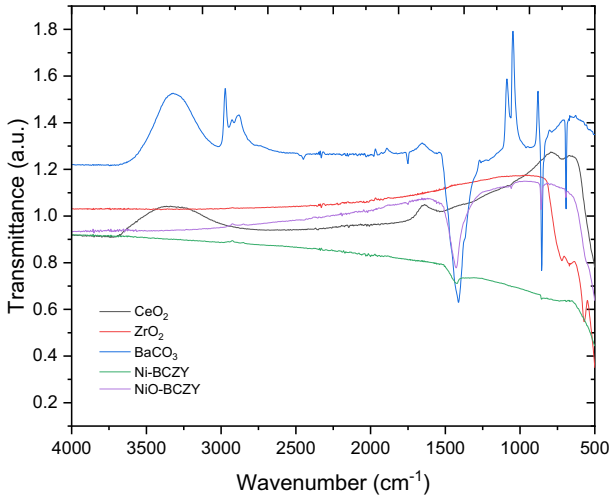

Fig. 2 – FT-IR spectra of the Ni-BZCY catalyst before and after reduction.

weaker in reduced Ni-BZCY sample, the possible reason is that, during the reduction process, the generated Ni particles diffuse and coat on the surface of $BaCO_3$ particles thus IR absorption for $BaCO_3$ is reduced. The decomposition of the trace amount of $BaCO_3$ is unlikely as the sample was prepared at 1000 °C which is 300 °C higher than the reducing temperature.

SEM observation

Fig. 3a and b show the SEM pictures of unreduced NiO-BZCY catalyst. The big particles are BZCY oxide with small NiO particles homogeneously distributed in the oxide matrix. The secondary particle size of NiO was about 0.2 μm (Fig. 3a). After high temperature reduction, the particle size of generated Ni particles was about 1.5 μm Ni (Fig. 3b), due to coarsening of Ni particles during the high temperature reduction. The particle size of Ni did not exhibit significant increase during the long time stability test (Fig. 3c). The increased intensity of Ni component in XRD is more likely due to better crystallisation during the high temperature operation. Element mapping of reduced Ni-BZCY is shown in Fig. 4. The distribution of Ni (Fig. 4b) and other elements is homogeneous. From Fig. 5 the particle size of Ni in Ni-BZCY and Ni–MgO–CeO_2 was compared, from this it was observed that a similar Ni particle size was achieved over both catalysts despite the large difference in particle size observed between BZCY and MgO–CeO_2. The particle size of MgO–CeO_2 prepared at 500 °C is much smaller than that of BZCY prepared at 1000 °C. This is consistent with the specific surface area for Ni-BZCY (0.907 $m^2\ g^{-1}$) and Ni–MgO–CeO_2 (16.940 $m^2\ g^{-1}$) measured by BET method.

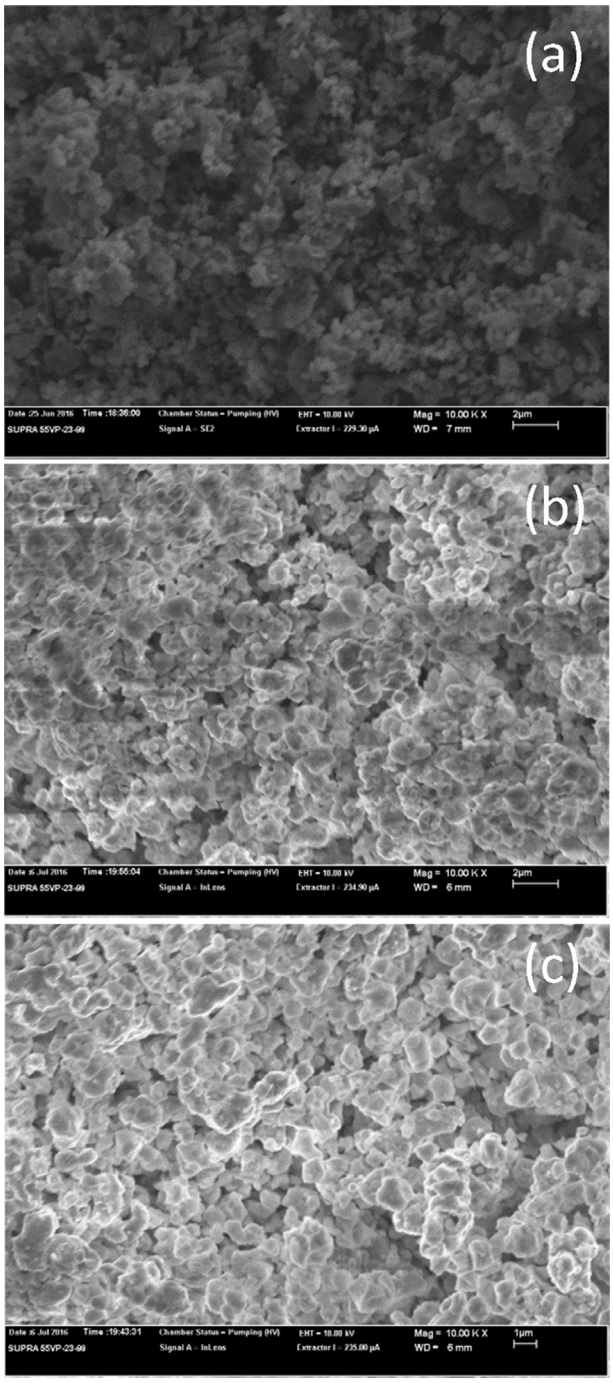

Fig. 3 – SEM images of the unreduced catalyst (a), the reduced catalyst before stability test (b) and the reduced catalyst after stability test (c). The magnification factor was 10000.

TG-DSC analysis

In order to figure out the effects of moisture on the properties of the reduced Ni-BZCY catalyst, TG-DSC analyses were carried out for both dry and wet reduced Ni-BZCY catalysts. For the wet catalyst, reduced Ni-BZCY catalyst was exposed to flowing air through room temperature for 1 h before the TG-DSC measurement. The TG-DSC data for both samples are shown below in Fig. 6(a) and (b) respectively. For the dry catalyst, the initial weight loss below 100 °C (~0.12 wt%) is due to the loss of absorbed water. When the wet reduced Ni-BZCY was used, the initial weight loss continued to ~250 °C, with a larger weight loss (~0.34 wt%) indicating BZCY can hold water to a higher temperature. A shoulder weight gain peaked around 450 °C was observed which is due to water uptake. This was also observed in protonic conducting oxides [44,45]. On cooling, more water uptake (~0.18 wt%) was observed

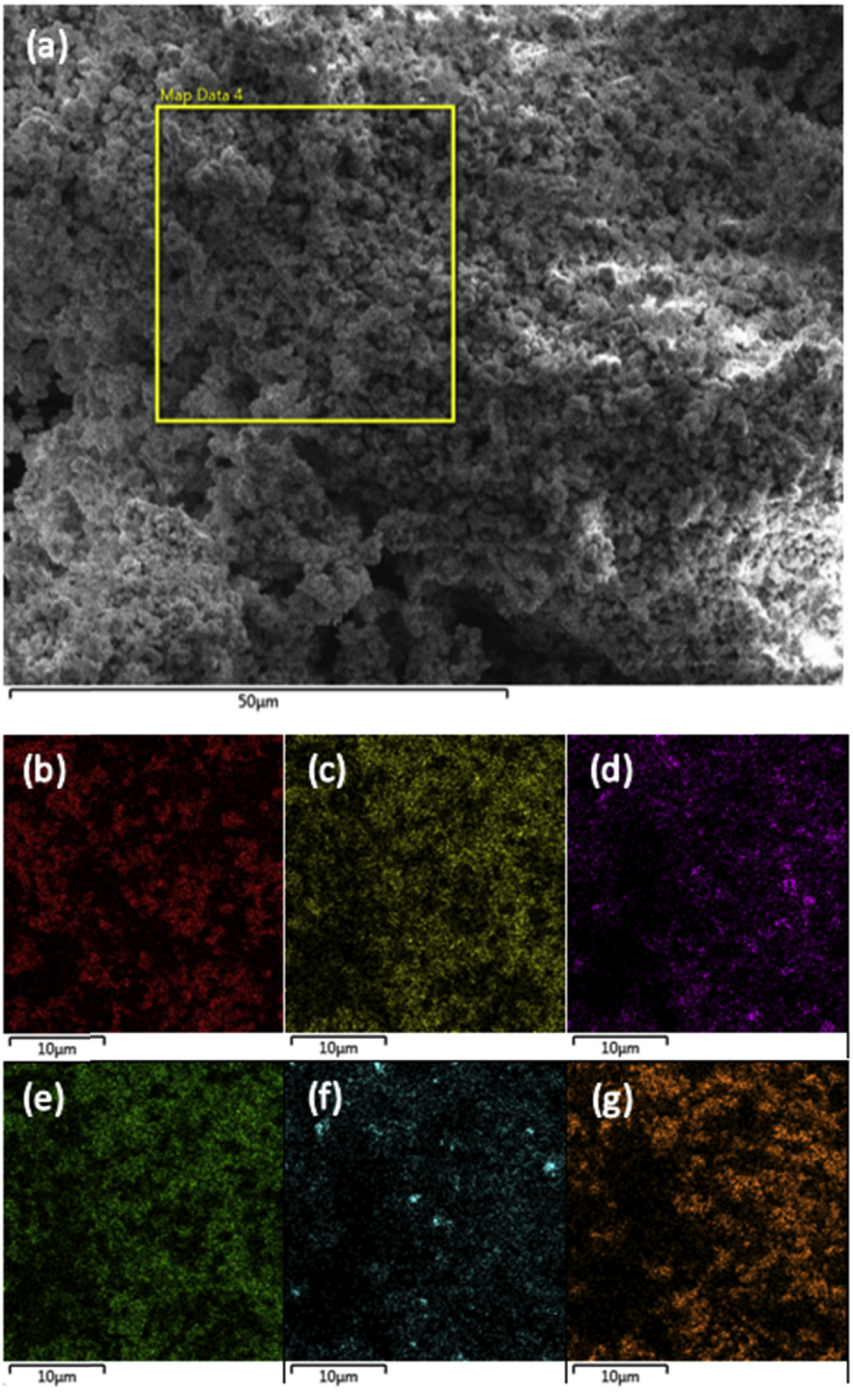

Fig. 4 – SEM image of the reduced catalyst before stability test with highlighted area of element mapping (a), EDS mapping for Ni (b), EDS mapping for Ba (c), EDS mapping for Zr (d), EDS mapping for Ce (e), EDS mapping for Y (f), EDS mapping for O (g).

indicating BZCY can strongly uptake water at lower temperatures. On the DSC curves, it has been noticed that there is an endothermic shoulder peak with positive thermal effect (on right Y-axis) has been observed peaked at around 625 °C for both samples which is related to the slow desorption of water. The observed weight and thermal effects are consistent with those in previous reports [44,45].

Catalytic activity towards ammonia synthesis

Effect of temperature on catalyst activity

When a constant flow rate was kept at 120 mL min^{-1} and H_2:N_2 were flown with a mole ratio of 3:1 the effects of changing temperature could be observed, this is shown in Fig. 7. It was observed that the activity increases up to a maximum of approximately 135 μmol g^{-1} h^{-1} at 620 °C before dropping

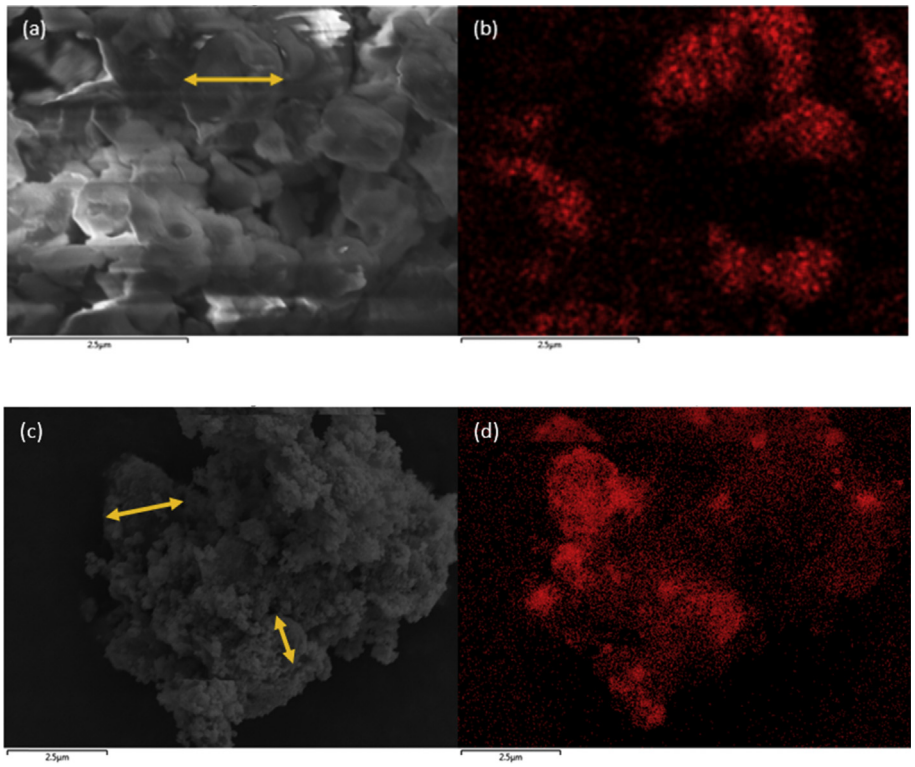

Fig. 5 – SEM image of: Ni-BZCY catalyst before stability test highlighting the particle size of the reduced Ni (a), EDS mapping for Ni on Ni-BZCY catalyst (b), Ni–MgO–CeO_2 catalyst before stability test highlighting the particle size of the reduced Ni (c), EDS mapping for Ni on Ni–MgO–CeO_2 catalyst.

again. At lower temperature, the catalytic activity of the Ni-BZCY catalyst is not high enough. At a higher temperature, the produced ammonia may decompose due to the thermodynamic equilibrium for the reaction shifting to the left as the reaction is exothermic, leading to lower production rate. In Fig. 6b, a weight loss at ~650 °C was observed due to the loss of uptaken water. This temperature is very close to the highest catalytic activity as shown in Fig. 7. Therefore promotion effect of the BZCY could be related to the uptaken water at high temperature. This trend was also observed by Vasileiou E et al. [1] in their cell when hydrogen and nitrogen were fed to the Ni – $BaZr_{0.7}Ce_{0.2}Y_{0.1}O_{3-\delta}$ electrode under open circuit conditions.

The ammonia outlet concentration was plotted alongside the equilibrium concentration for the reaction in Fig. 8. Thermodynamic equilibrium data was obtained from Haber's Nobel Lecture [46]. It can be observed that the outlet concertation reaches a maximum and starts to decrease before obtaining the outlet concertation expected at thermodynamic equilibrium. It is therefore expected that the activity over 620 °C is inhibited due to some other means. The outlet concentration of ammonia at 700 °C was still closer to the thermodynamic equilibrium than those at lower temperatures.

Effect of total flow rate on catalyst activity

The effect of total flow rate was then tested at a constant temperature of 620 °C with the results shown in Fig. 9. It can be seen that the activity increases with increasing flow rate. This increase in activity expected to be due solely to the increase in reactant gas, in order to confirm this ammonia outlet concentration was plotted against total gas flow rate.

As shown in Fig. 10, when total flow rate is plotted against ammonia outlet concentration, it rises up to a total flow rate of 120 mL min^{-1} before levelling off. The outlet concentration was calculated using the following equation

$$Outlet\ NH3\ concentraion = \frac{r_{NH_3} \times m}{Total\ molar\ flowrate} \times 100\% \quad (10)$$

This therefore shows that the total flow rate is independent of conversion rate over a value of 120 mL min^{-1} in our experiments and that the activity measured at this these flow rates is solely due to catalytic activity. However, at total gas flow rates less than 120 mL min^{-1}, lower outlet ammonia concentration was observed. The possible reason is that, majority of the mixed gas passed through the edge of the glass fibre where the loading of catalyst was relatively lower thus the contact time with the catalyst was short leading to reduced ammonia formation.

Effect of feed gas ratio on catalyst activity

To determine the optimal feed ratio the gas inlet mole ratio was adjusted area when 2.6 and 3.4 (H_2/N_2) with the optimal being detected for a value of 3.2 with a rate of approximately 320 μmol g^{-1} h^{-1} (Fig. 11). All measurements were taken at 620 °C with a total flow rate of 200 ml/min. The reason for this deviation from the normal may be due to the proton conducting nature of the BZCY support with some of the fed H_2

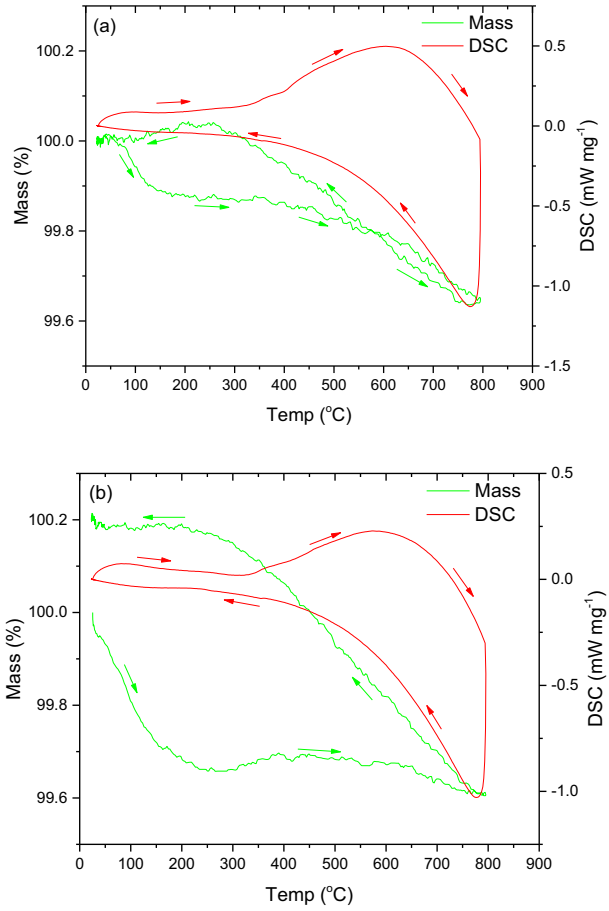

Fig. 6 – (a): STA analysis of dry Ni-BZCY in N_2 (b): STA analysis of wet Ni-BZCY in N_2.

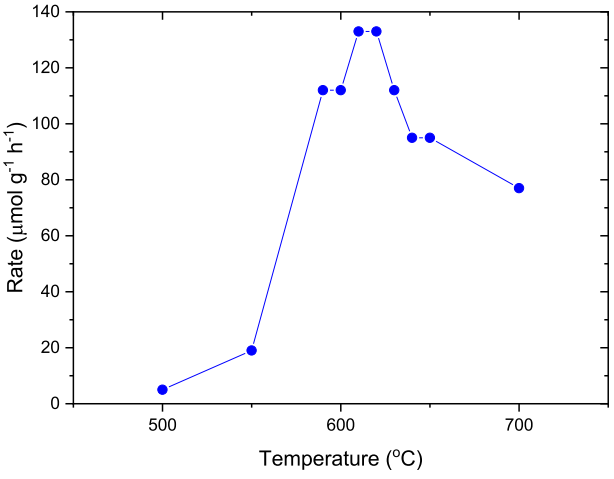

Fig. 7 – Ammonia synthesis rate using a Ni-BZCY catalyst at different temperatures (120 mL min^{-1}, H_2:N_2 = 3:1).

being ionised and transferred to the support as H^+ therefore adjusting the value of H_2 to N_2 in the reactor closer to the stoichiometric value of 3. This phenomenon of a H^+ being transferred to the active sites was observed by Shin H et al. [47] when they used proton conducting support materials for a Cr catalyst in the degradation of ethane.

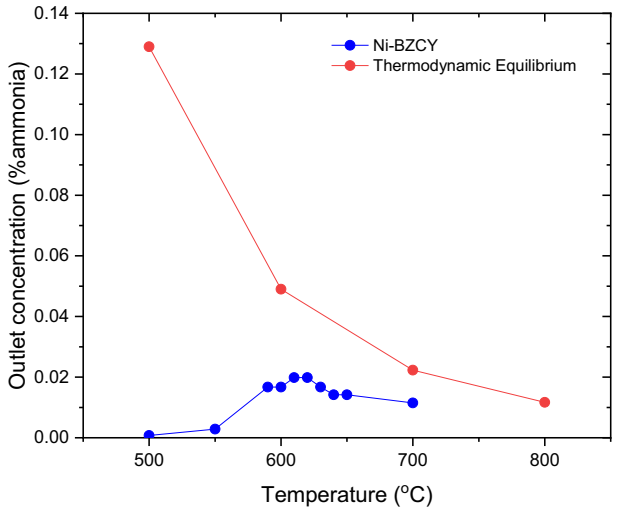

Fig. 8 – Ammonia outlet concentration of Ni-BZCY catalyst compared to thermodynamic equilibrium (120 mL min^{-1}, H_2:N_2 = 3:1, 1 bar).

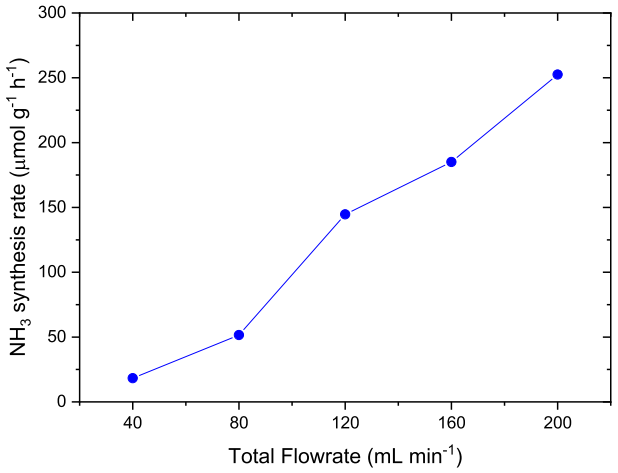

Fig. 9 – Ammonia synthesis rate using a Ni-BZCY catalyst at different flow rates (620 °C, H_2:N_2 = 3:1).

Effect of temperature on catalyst activity of Ni/MgO–CeO_2

In order to examine the promotion effects of the proton conducting nature of the catalyst support, a Ni catalyst supported on a non-proton conductor was tested under the same conditions. It has been reported that MgO–CeO_2 composite is an excellent support for Ru catalysts for ammonia synthesis [48]. In this study, for comparison, Ni supported in MgO–CeO_2 composite was also synthesised and the catalytic activity was also investigated. This was tested over the temperature range of 600 °C–640 °C with a hydrogen to nitrogen mole ratio of 3 and a total flow rate of 120 mL min^{-1} (Fig. 12). From this it can be seen that the maximum flow rate achieved was at 620 °C mirroring that results obtained for the BZCY support. However, the activity of this catalyst is around 4 times lower than the activity of the Ni catalyst when used with the BZCY proton conducting support (Fig. 7). However, the catalytic activity is related to the specific surface area. The specific surface area was measured to be 0.907 m^2 g^{-1} for the Ni-BZCY catalyst and

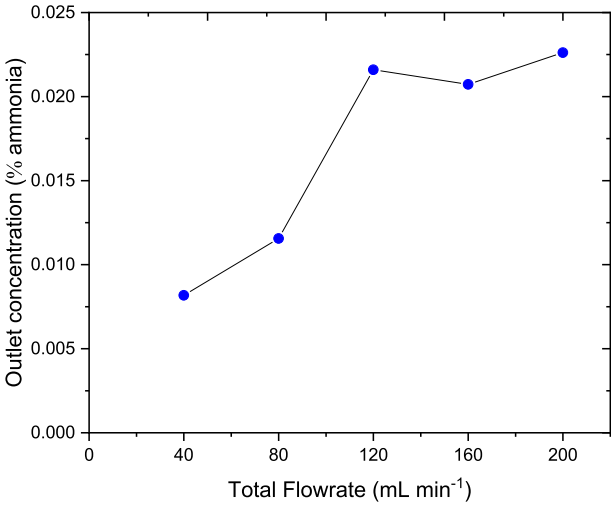

Fig. 10 – Ammonia outlet concentration at different flow rates (620 °C, H_2:N_2 = 3:1).

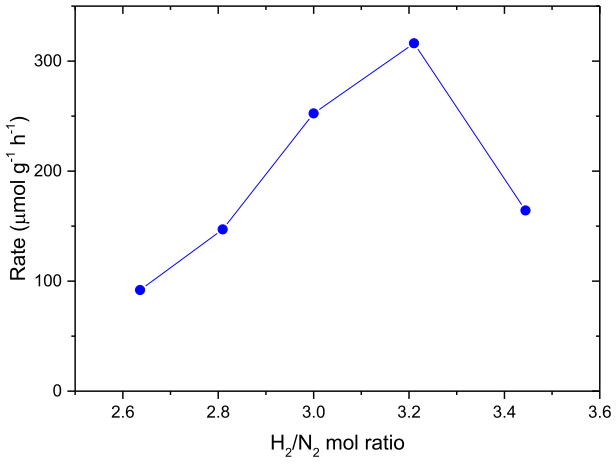

Fig. 11 – Ammonia synthesis rate using a Ni-BZCY catalyst at different feed mole ratios (200 mL min^{-1}, 620 °C).

16.940 m^2 g^{-1} for the Ni–MgO–CeO_2 catalyst. The specific surface area of Ni-BZCY is only 5.3% of that of Ni–MgO–CeO_2 but the catalytic activity to ammonia synthesis is much higher, with a specific activity of approximately 149 μmol m^{-2} h^{-1} for the Ni-BZCY catalyst compared to 2 μmol m^{-2} h^{-1} for the Ni–MgO–CeO_2 catalyst. This experiment further demonstrates that proton-conducting oxide BZCY has obvious promotion effects on ammonia synthesis.

Stability of catalytic activity in the presence of moisture

The stability of ammonia synthesis catalysts in the presence of an oxidant is a big challenge [12,19]. It has been reported that Ru–Y_5Si_3 catalyst exhibit good stability in the presence of moisture [21]. Inspired by this excellent work, we also investigated the stability of our catalysts in the same manner. The catalyst stability was investigated over 144 h at 620 °C with a H_2/N_2 mole ratio of 3 and a total flow rate of 200 mL min^{-1}. The catalyst was found to be stable over this period with no loss of activity as can be seen in Fig. 13. After this the effect of wetting

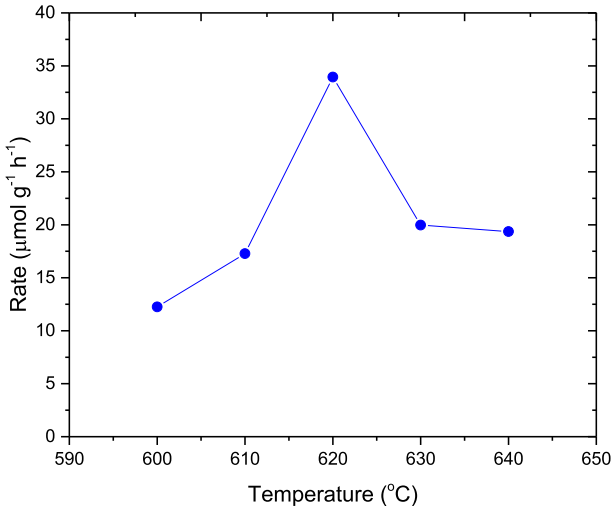

Fig. 12 – Ammonia synthesis rate using 60%NiO/40%MgO–CeO_2 catalyst at different temperatures (120 mL min^{-1}, H_2:N_2 = 3:1).

the catalyst was also investigated. To perform these experiments the reactor was cooled to room temperature and wet nitrogen (100 mL min^{-1}) was bubbled through the reactor for 1 h before being heated back to 620 °C at a rate of 1 °C min^{-1}. This was repeated 5 times with the results shown in Fig. 13. It can be seen from the results that there is a drop in activity after each cycle with an overall linear drop over the 5 cycles. The activity drops to approximately a fifth of its original value after 5 cycles going from approximately 250 μmol g^{-1} h^{-1} to 50 μmol g^{-1} h^{-1} with a further drop expected on further wetting cycles. This loss of activity was suspected to be caused either due to the poisoning effect of the water on the Ni catalyst after being wetted at room temperature because slight oxidation of Ni on the surface may happen as the case for Fe-based catalysts [12]. However, upon examining the XRD patterns and SEM images of the reduced catalyst after the stability test no major changes in particle size were observed from the freshly reduced catalyst (Fig. 3b and c). However, a trace amount of NiO may still have been formed after treating the catalyst but is beyond the measurement limit for XRD. This NiO will be *in situ* reduced to metallic Ni at high temperature in the presence of high concentration of H_2. The oxidation and reduction cycles that the Ni catalyst undergoes in the wetted catalyst may also damage the active sites on the catalyst greatly speeding up the degradation of the catalyst that would be noticed over the catalysts life time [49], evidence for this was observed during the XRD which showed an increase in intensity of the Ni peak after the stability test suggesting possible better crystallisation of Ni particle leading to loss of active sites on the Ni surface. This effect of enhanced catalyst degradation may also be attributed to the heating and cooling cycles in-between each data point on the wetted catalyst stability test.

As well as the BZCY promoted catalyst pure Ni was also tested with a rate of 25.12 μmol g^{-1} h^{-1} observed at 620 °C with a total flow rate of 200 mL/min and a H_2/N_2 ratio of 3. This is roughly ten times lower than that for the BZCY promoted catalyst when the same weight of nickel oxide was used. This

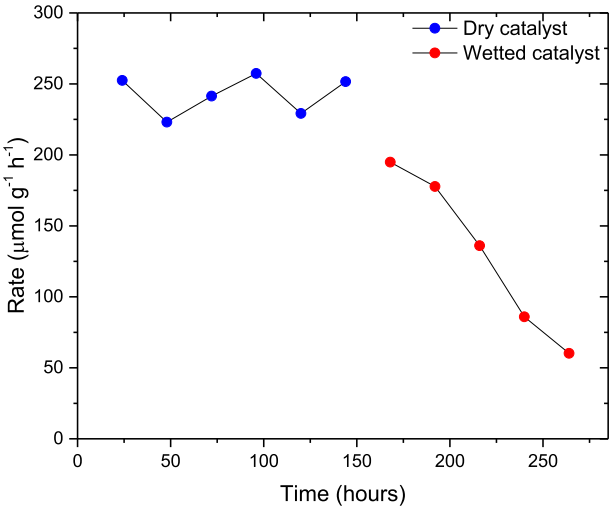

Fig. 13 – Ammonia synthesis rate using a Ni-BZCY catalyst over dry and wet stability tests (620 °C, 200 mL min^{-1}, H_2:N_2 = 3:1).

therefore shows the excellent promotion effects that can be achieved using the BZCY proton conducting support.

When investigating materials as potential supports for ammonia synthesis catalysts the electro negativity of the support is a strong consideration [50–52]. It has been shown that the electron transferring nature of support could be attributed to increased activity [50–52]. This is mainly prominent in Ru catalyst supports where the transferred electrons change the electronic state of the Ru catalyst [53]. However, in this work, we have shown that another desirable effect of a support material may be its ability to conduct protons. This promoting ability of proton conducting supports could be explained by the ionisation of the H_2 gas fed to the reactor. It is commonly accepted that the rate limiting step for the ammonia synthesis reaction is the dissociation of the N_2 molecules on the catalyst surface [54,55] or the N-binding for Fe catalysts; however, if molecular H_2 is adsorbed on the catalyst active sites instead then the catalytic activity would suffer due the loss of active sites for the rate limiting step [56]. By using a proton conducting support it is suggested that the dissociated hydrogen on the active sites is then transferred in to the support freeing the site for the adsorption of nitrogen. The dissociated nitrogen on the active sights may then further react with the H^+ ions in the support further increasing activity. It has been reported that the active sites for CO_2 reduction on Cu from reduced CuO is mainly on the grain boundary whist the well crystallized BZCY has higher promotion activity that less crystallised MgO–CeO_2 support [57]. This could be related to the proton conduction of BZCY. Other possibilities such as lattice mismatch or metal/metal-oxide support interactions/adhesion cannot be ruled out, which need further investigation. Anyway, the reaction mechanisms on CO_2 reduction and N_2 reduction are very different and hard to compare. Despite these promotion effects, the reaction temperature is too high for any meaningful application of the reported catalyst; however, the excellent promotion effects of the proton conducting support has been shown with the activity increasing by an order of magnitude. It is therefore expected that when used with more conventional catalysts such as Ru, Co or Fe then high activities at lower temperatures more in line with those employed in the Haber - Bosch process can be achieved.

Conclusion

The use of a BZCY proton conducting support has proven to increase the activity of Ni towards ammonia synthesis by an order of magnitude. This increase in activity was observed even though no gas purification was employed. At 620 °C and a total flow rate of 200 mL min^{-1} it was observed that an ammonia synthesis rate of approximately 250 μmol g^{-1} h^{-1} could be achieved which is ten times higher than that observed for unpromoted nickel under the same conditions. The activity of Ni supported on proton-conducting oxide $BaZr_{0.1}Ce_{0.7}Y_{0.2}O_{3-\delta}$ is four times of that of Ni supported on non-proton conductor MgO–CeO_2 although the specific surface area of the former is much lower, giving a specific activity of around 72 times lower than that of Ni supported on $BaZr_{0.1}Ce_{0.7}Y_{0.2}O_{3-\delta}$. The observed activity of the promoted Ni catalysts is slightly lower than the known Fe and Ru based catalyst at 400–500 °C and a pressure of one atmosphere because Ni itself is not a good ammonia synthesis catalyst [21,58,59]. It is therefore expected that when employed with more active catalysts such as Fe, Co or Ru then an increase in activity could be achieved which we believe is tied to the proton conducting nature of the support. The relevant research are on-going in our group.

Acknowledgements

The authors thank EPSRC (Grant No. EP/G01244X/1) and Innovate UK (Grant No. 104010 and 133714) for funding. One of the authors (Humphreys) would like to thank the University of Warwick for a DTG PhD studentship.

REFERENCES

[1] Apodaca LE. Nitrogen (fixed) – ammonia. In: Survey USG. United States: United States Geological Survey Publication; 2014. p. 2.
[2] Erisman JW, Sutton MA, Galloway J, Klimont Z, Winiwarter W. How a century of ammonia synthesis changed the world. Nat Geosci 2008;1:636–9.
[3] Lan R, Irvine JTS, Tao SW. Ammonia and related chemicals as potential indirect hydrogen storage materials. Int J Hydrogen Energy 2012;37:1482–94.
[4] Lan R, Alkhazmi KA, Amar IA, Tao SW. Synthesis of ammonia directly from wet air using $Sm_{0.6}Ba_{0.4}Fe_{0.8}Cu_{0.2}O_{3-\delta}$ as the catalyst. Faraday Discuss 2015;182:353–63.
[5] Yun DS, Joo JH, Yu JH, Yoon HC, Kim J-N, Yoo C-Y. Electrochemical ammonia synthesis from steam and nitrogen using proton conducting yttrium doped barium zirconate electrolyte with silver, platinum, and lanthanum

strontium cobalt ferrite electrocatalyst. J Power Sources 2015;284:245–51.
[6] Lan R, Alkhazmi KA, Amar IA, Tao S. Synthesis of ammonia directly from wet air using new perovskite oxide $La_{0.8}Cs_{0.2}Fe_{0.8}Ni_{0.2}O_{3-\delta}$ as catalyst. Electrochim Acta 2014;123:582–7.
[7] Amar IA, Lan R, Petit CTG, Tao SW. Solid-state electrochemical synthesis of ammonia: a review. J Solid State Electrochem 2011;15:1845–60.
[8] Amar IA, Lan R, Humphreys J, Tao SW. Electrochemical synthesis of ammonia from wet nitrogen via a dual-chamber reactor using $La_{0.6}Sr_{0.4}Co_{0.2}Fe_{0.8}O_{3-\delta}$-$Ce_{0.8}Gd_{0.18}Ca_{0.02}O_{2-\delta}$ composite cathode. Catal Today 2017;286:51–6.
[9] Fan L, Wang C, Chen M, Zhu B. Recent development of ceria-based (nano)composite materials for low temperature ceramic fuel cells and electrolyte-free fuel cells. J Power Sources 2013;234:154–74.
[10] Shimoda N, Kimura Y, Kobayashi Y, Kubota J, Satokawa S. Ammonia synthesis over yttrium-doped barium zirconate and cerate-based perovskite-type oxide supported ruthenium. catalysts. Int J Hydrogen Energy 2017;42:29745–55.
[11] Kishira S, Qing G, Suzu S, Kikuchi R, Takagaki A, Oyama ST. Ammonia synthesis at intermediate temperatures in solid-state electrochemical cells using cesium hydrogen phosphate based electrolytes and noble metal catalysts. Int J Hydrogen Energy 2017;42:26843–54.
[12] Liu H. Ammonia synthesis catalyst 100 years: practice, enlightenment and challenge. Chin J Catal 2014;35:1619–40.
[13] Han W, Huang S, Cheng T, Tang H, Li Y, Liu H. Promotion of Nb_2O_5 on the wustite-based iron catalyst for ammonia synthesis. Appl Surf Sci 2015;353:17–23.
[14] Yu XJ, Lin BY, Lin JX, Wang R, Wei KM. A novel fused iron catalyst for ammonia synthesis promoted with rare earth gangue. J Rare Earths 2008;26:711–6.
[15] Hagen S, Barfod R, Fehrmann R, Jacobsen CJH, Teunissen HT, Chorkendorff I. Ammonia synthesis with barium-promoted iron–cobalt alloys supported on carbon. J Catal 2003;214:327–35.
[16] Brown DE, Edmonds T, Joyner RW, McCarroll JJ, Tennison SR. The genesis and development of the commercial BP doubly promoted catalyst for ammonia synthesis. Catal Lett 2014;144:545–52.
[17] Huo C, Xia Q-H, Pan M-H, Liu H-Z. Efficient La-Ba-MgO supported Ru catalysts for ammonia synthesis. Catal Lett 2011;141:1275–81.
[18] Lin B, Wang R, Lin J, Ni J, Wei K. Effect of chlorine on the chemisorptive properties and ammonia synthesis activity of alumina-supported Ru catalysts. Catal Lett 2011;141:1557–68.
[19] Liu H. Ammonia synthesis catalysts innovation and practice. World Scientific Publishing Co and Chemical industry press; 2013.
[20] Inoue Y, Kitano M, Kim SW, Yokoyama T, Hara M, Hosono H. Highly dispersed Ru on electride Ca24Al28O64 (4+)(e(-))(4) as a catalyst for ammonia synthesis. ACS Catal 2014;4:674–80.
[21] Lu Y, Li J, Tada T, Toda Y, Ueda S, Yokoyama T, et al. Water durable electride Y_5Si_3: electronic structure and catalytic activity for ammonia synthesis. J Am Chem Soc 2016;138:3970–3.
[22] Wang Z, Lin J, Wang R, Wei K. Ammonia synthesis over ruthenium catalyst supported on perovskite type $BaTiO_3$. Catal Commun 2013;32:11–4.
[23] Wang Z, Liu B, Lin J. Highly effective perovskite-type BaZrO3 supported Ru catalyst for ammonia synthesis. Appl Catal Gen 2013;458:130–6.
[24] Vojvodic A, Medford AJ, Studt F, Abild-Pedersen F, Khan TS, Bligaard T, et al. Exploring the limits: a low-pressure, low-temperature Haber–Bosch process. Chem Phys Lett 2014;598:108–12.
[25] van der Ham CJM, Koper MTM, Hetterscheid DGH. Challenges in reduction of dinitrogen by proton and electron transfer. Chem Soc Rev 2014;43:5183–91.
[26] Marnellos G, Stoukides M. Ammonia synthesis at atmospheric pressure. Science 1998;282:98–100.
[27] Marnellos G, Karagiannakis G, Zisekas S, Stoukides M. Electrocatalytic synthesis of ammonia at atmospheric pressure. In: Avelino Corma FVMSM, José Luis GF, editors. Studies in surface science and catalysis. Elsevier; 2000. p. 413–8.
[28] Murakami T, Nishikiori T, Nohira T, Ito Y. Electrolytic synthesis of ammonia in molten salts under atmospheric pressure. J Am Chem Soc 2003;125:334–5.
[29] Murakami T, Nohira T, Goto T, Ogata YH, Ito Y. Electrolytic ammonia synthesis from water and nitrogen gas in molten salt under atmospheric pressure. Electrochim Acta 2005;50:5423–6.
[30] Garagounis I, Kyriakou V, Skodra A, Vasileiou E, Stoukides M. Electrochemical synthesis of ammonia in solid electrolyte cells. Front Energy Res 2014;2:1–10.
[31] Giddey S, Badwal SPS, Kulkarni A. Review of electrochemical ammonia production technologies and materials. Int J Hydrogen Energy 2013;38:14576–94.
[32] Licht S, Cui B, Wang B, Li F-F, Lau J, Liu S. Ammonia synthesis by N_2 and steam electrolysis in molten hydroxide suspensions of nanoscale Fe_2O_3. Science 2014;345:637–40.
[33] Lan R, Irvine JTS, Tao SW. Synthesis of ammonia directly from air and water at ambient temperature and pressure. Sci Rep 2013;3:1145.
[34] Lan R, Alkhazmi KA, Amar IA, Tao SW. Synthesis of ammonia directly from wet air at intermediate temperature. Appl Catal B Environ 2014;152–153:212–7.
[35] Lan R, Tao SW. A simple high performance matrix-free biomass molten carbonate fuel cell without CO_2 recirculation. Sci Adv 2016;2:e1600772.
[36] Vasileiou E, Kyriakou V, Garagounis I, Vourros A, Stoukides M. Ammonia synthesis at atmospheric pressure in a $BaCe_{0.2}Zr_{0.7}Y_{0.1}O_{2.9}$ solid electrolyte cell. Solid State Ionics 2015;275:110–6.
[37] Vasileiou E, Kyriakou V, Garagounis I, Vourros A, Manerbino A, Coors WG, et al. Reaction rate enhancement during the electrocatalytic synthesis of ammonia in a $BaZr_{0.7}Ce_{0.2}Y_{0.1}O_{2.9}$ solid electrolyte cell. Top Catal 2015;58:1193–201.
[38] Zhang Y, Zha S, Liu M. Dual-scale porous electrodes for solid oxide fuel cells from polymer foams. Adv Mater 2005;17:487–91.
[39] Sun W, Tao Z, Shi Z, Yan L, Zhu Z, Liu W. Fabrication of $BaZr_{0.1}Ce_{0.7}Y_{0.2}O_{3-\delta}$-based proton-conducting solid oxide fuel cells Co-fired at 1,150 °C. Fuel Cell 2010;10:1108–13.
[40] Fang SM, Brinkman KS, Chen FL. Hydrogen permeability and chemical stability of Ni-$BaZr_{0.1}Ce_{0.7}Y_{0.1}Yb_{0.1}O3$-δ membrane in concentrated H_2O and CO_2. J Membr Sci 2014;467:85–92.
[41] Fang S, Brinkman K, Chen F. Unprecedented CO_2-promoted hydrogen permeation in Ni-$BaZr_{0.1}Ce_{0.7}Y_{0.1}Yb_{0.1}O_{3-\delta}$ membrane. ACS Appl Mater Interfaces 2014;6:725–30.
[42] Tipcompor N, Thongtem T, Phuruangrat A, Thongtem S. Characterization of SrCO3 and BaCO3 nanoparticles synthesized by cyclic microwave radiation. Mater Lett 2012;87:153–6.
[43] Cervera RB, Oyama Y, Miyoshi S, Kobayashi K, Yagi T, Yamaguchi S. Structural study and proton transport of bulk nanograined Y-doped BaZrO3 oxide protonics materials. Solid State Ionics 2008;179:236–42.
[44] Xu XX, Tao SW, Irvine JTS. Proton conductivity of potassium doped barium zirconates. J Solid State Chem 2010;183:93–8.

[45] Kreuer KD. Proton-conducting oxides. Annu Rev Mater Res 2003;33:333–59.
[46] Haber F. The synthesis of ammonia from its elements Nobel lecture, June 2, 1920. Resonance 2002;7:86–94.
[47] Shin HH, McIntosh S. Proton-conducting perovskites as supports for Cr catalysts in short contact time ethane dehydrogenation. ACS Catal 2015;5:95–103.
[48] Saito M, Itoh M, Iwamoto J, Li C-Y, Machida K-i. Synergistic effect of MgO and CeO_2 as a support for ruthenium catalysts in ammonia synthesis. Catal Lett 2006;106:107–10.
[49] Huttig GF. Catalytic activity and composition of oxide systems. Discuss Faraday Soc 1950;8:215–22.
[50] You Z, Inazu K, Aika K-i, Baba T. Electronic and structural promotion of barium hexaaluminate as a ruthenium catalyst support for ammonia synthesis. J Catal 2007;251:321–31.
[51] Seetharamulu P, Hari Prasad Reddy K, Padmasri AH, Rama Rao KS, David Raju B. Role of promoters on highly active nano-Ru catalyst supported on Mg–Al hydrotalcite precursor for the synthesis of ammonia. Catal Today 2009;141:94–8.
[52] Lin J, Wang Z, Zhang L, Ni J, Wang R, Wei K. Ammonia synthesis over ruthenium catalysts using barium-doped zirconia as supports prepared by citric acid method. Chin J Catal 2012;33:1075–9.
[53] Wang X, Ni J, Lin B, Wang R, Lin J, Wei K. Highly efficient Ru/MgO–CeO_2 catalyst for ammonia synthesis. Catal Commun 2010;12:251–4.
[54] Stoltze P, Norskov JK. Bridging the pressure gap between ultrahigh-vacuum surface physics and high-pressure catalysis. Phys Rev Lett 1985;55:2502–5.
[55] Vandervell HD, Waugh KC. On the role of promoters in promoted iron catalysts used in the industrial synthesis of ammonia. Chem Phys Lett 1990;171:462–8.
[56] Bowker M, Parker IB, Waugh KC. Extrapolation of the kenitics of model ammonia-synthesis catalysts to industrially relevant temperatures and pressures. Appl Catal 1985;14:101–18.
[57] Li CW, Kanan MW. CO2 reduction at low overpotential on Cu electrodes resulting from the reduction of thick Cu2O films. J Am Chem Soc 2012;134:7231–4.
[58] Zeng HS, Inazu K, Aika K. The working state of the barium promoter in ammonia synthesis over an active-carbon-supported ruthenium catalyst using barium nitrate as the promoter precursor. J Catal 2002;211:33–41.
[59] Kitano M, Inoue Y, Yamazaki Y, Hayashi F, Kanbara S, Matsuishi S, et al. Ammonia synthesis using a stable electride as an electron donor and reversible hydrogen store. Nat Chem 2012;4:934–40.